The Astrophysical Journal, 760:18 (8pp), 2012 November 20 doi:10.1088/0004-637X/760/1/18

THE EXTREME-ULTRAVIOLET EMISSION FROM SUN-GRAZING COMETS

P. Bryans[1] and W. D. Pesnell[2]
[1] ADNET Systems Inc., NASA Goddard Space Flight Center, Code 671, Greenbelt, MD 20771, USA
[2] NASA Goddard Space Flight Center, Code 671, Greenbelt, MD 20771, USA
Received 2012 June 7; accepted 2012 September 25; published 2012 October 30

ABSTRACT

The Atmospheric Imaging Assembly (AIA) on the *Solar Dynamics Observatory* has observed two Sun-grazing comets as they passed through the solar atmosphere. Both passages resulted in a measurable enhancement of extreme-ultraviolet (EUV) radiance in several of the AIA bandpasses. We explain this EUV emission by considering the evolution of the cometary atmosphere as it interacts with the ambient solar atmosphere. Molecules in the comet rapidly sublimate as it approaches the Sun. They are then photodissociated by the solar radiation field to create atomic species. Subsequent ionization of these atoms produces a higher abundance of ions than normally present in the corona and results in EUV emission in the wavelength ranges of the AIA telescope passbands.

Key words: comets: general – comets: individual (C/2011 N3, C/2011 W3) – Sun: corona – Sun: general

Online-only material: color figures

1. INTRODUCTION

Thousands of Sun-grazing comets have been detected since the advent of space-based solar observation. The most successful instrument for observing these has been the Large Angle and Spectrometric Coronagraph (LASCO; Brueckner et al. 1995) on the *Solar and Heliospheric Observatory* (*SOHO*; Domingo et al. 1995), which has observed more than 2000 such comets approaching the Sun (see, e.g., Biesecker et al. 2002; Knight et al. 2010). For a complete catalog of Sun-grazing comets, see the US Naval Research Laboratory *Sungrazing Comets* Web site.[3] Very few Sun-grazing comets have been seen to survive their close passage to the solar photosphere and emerge post perihelion (Marsden 2005), none of which has been observed by LASCO until 2011.[3]

Despite the lack of direct observation of the destruction of a Sun-grazing comet, the literature is not lacking in predictions of the results of such an event. It is not possible to give a full literature review here, but we highlight some papers of particular relevance. Weissman (1983) and Sekanina (1984) discussed the physical processes of import to the destruction of comets during their perihelion passage. A more complete model detailing the erosion of Sun-grazing comets was presented by Sekanina (2003). And, most recently, Brown et al. (2011) have provided analytical models describing the destruction mechanism of Sun-grazing and -impacting comets. This latter work indicates that the dominant mass-loss mechanism varies between sublimation, ablation, and explosion depending on the cometary mass and perihelion distance. One particularly interesting prediction is that a Sun-impacting comet large enough to reach the chromosphere would result in solar-flare-like energy release.

Further from the Sun, it has been known for around 15 years that comets emit at X-ray and extreme-ultraviolet (EUV) wavelengths. In 1996, comet C/1996 B2 (Hyakutake) was observed by the *ROSAT* X-ray telescope (Lisse et al. 1996). Subsequently, all comets within 3 AU were found to emit X-rays (Dennerl et al. 1997). The discovery of this emission was initially surprising, given the low temperature of the cometary atmosphere, but was explained as arising from charge exchange between solar wind ions and neutral cometary species (Cravens 1997; Krasnopolsky 1997). However, until 2011, there had been no observations of a Sun-grazing comet close to perihelion, let alone at such wavelengths.

The launch of the *Solar Dynamics Observatory* (*SDO*; Pesnell et al. 2012) in 2010 provides a unique capability to observe Sun-grazing comets. The Atmospheric Imaging Assembly (AIA; Lemen et al. 2012) images the entire Earth-facing solar corona at a cadence of 12 s with ∼1.2 arcsec resolution in seven EUV channels, with passbands centered at 94, 131, 171, 193, 211, 304, and 335 Å. Should a Sun-grazing comet be sufficiently bright in the EUV as it flies within the field of view of AIA, the high spatial and temporal resolution of AIA makes it the ideal instrument to observe such an event.

The first detection of a comet by *SDO* was on 2011 July 5–6, when comet C/2011 N3 (SOHO) passed across the disk of the Sun (Schrijver et al. 2012). It was detected in several of the AIA passbands before disappearing as it evaporated in the solar atmosphere. A second comet, C/2011 W3 (Lovejoy), was observed on 2011 December 15–16, this time passing behind the east limb of the solar disk and emerging on the west limb. Again, several of the AIA passbands detected EUV emission. As we will show below, cometary neutral species cannot survive very long at such close proximity to the solar radiation field. Thus, the explanation for EUV emission in Sun-grazing comets must differ from the charge-exchange model used to explain the X-ray emission detected in the heliosphere. This paper offers such an explanation.

The remainder of the paper is organized as follows. In Section 2, we describe the AIA observations of the two comets. In Section 3, we describe the model of the comet–corona interaction used to explain the EUV emission, including our simplified description of the cometary topology and the physical parameters of the cometary and solar atmospheres used in our calculations. Section 4 outlines the rate of evolution of the cometary material as it is sublimated from the comet body and subsequently dissociated and ionized in the corona. In Section 5, we show what contribution the cometary material has to EUV emission in the AIA channels. Finally, in Section 6 we give our conclusions and offer some suggestions on future work to improve our emission model.

[3] http://sungrazer.nrl.navy.mil/

2. OBSERVATIONS

2.1. Comet C/2011 N3 (SOHO)

Comet C/2011 N3 (SOHO) was first detected by the LASCO coronagraph in white light, approaching the west limb of the Sun. On 2011 July 5–6, it passed across the disk of the Sun and was detected by AIA (Schrijver et al. 2012). The first detection was in AIA 171 Å, off the solar limb, at 2011 July 5 23:46 UT, and was tracked until 2011 July 6 00:05:50 UT. Emission was also detected in the 131, 193, 211, and 335 Å passbands. The observations suggest that the comet may have fragmented before evaporating in the solar atmosphere.

Of the seven EUV channels of AIA, five show a response to the comet (Schrijver et al. 2012). There was no significant detection in the 94 or 304 Å channels; the 94 Å channel has a low signal-to-noise ratio in these observations and the 304 Å channel is dominated by the bright emission from lower in the solar atmosphere. The enhancement over the background emission is greatest in the 131 and 171 Å passbands, where the cometary emission is ∼10% above the background. However, the comet brightness was determined by summing over a box of 30×15 AIA pixels—a significantly larger area than the emitting region—so the true intensity enhancement due to the comet is greater.

2.2. Comet C/2011 W3 (Lovejoy)

A second comet, C/2011 W3 (Lovejoy), was observed by *SDO* on 2011 December 15. This passage of another Kreutz-family comet 5 months later resulted in perihelion being on the far side of the Sun from the perspective of *SDO*. Ground observations several days prior to perihelion gave an accurate estimate of the cometary orbit (Green 2011), allowing *SDO* to repoint 1250 arcsec east of solar center, giving extended observations of the comet as it approached the eastern limb. Comet C/2011 W3 (Lovejoy) was appreciably more massive than C/2011 N3 (SOHO), allowing it to survive perihelion and emerge on the other side of the Sun (see Gundlach et al. 2012 for a discussion on the survival). *SDO* had repointed to Sun center in time to observe the emergence. An in-depth analysis of the orbit can be found in Sekanina & Chodas (2012). We make particular note of the absence of observable cometary dust at the time of the AIA observations as a result of any dust particles being rapidly sublimated (Sekanina & Chodas 2012).

Despite perihelion passage being obscured by the solar disk, C/2011 W3 (Lovejoy) resulted in, perhaps, more interesting observations than C/2011 N3 (SOHO). The absence of contamination from background emission from the solar disk in the off-limb observations gives a clear picture of sublimated cometary material following the solar magnetic field. In contrast to C/2011 N3 (SOHO), C/2011 W3 (Lovejoy) produced significant signals in the 304 Å channel. For the channels that also detected C/2011 N3 (SOHO), the brightness contrast is similar in the C/2011 W3 (Lovejoy) observations.

Figure 1 shows the comet ingress in the 171, 131, and 304 Å wavelength channels of AIA. Two images at each wavelength are shown, separated by 1 minute, and nearly simultaneous across the three wavelength channels. Panels (a) and (b) show the 171 Å emission, where evidence of the cometary material following the magnetic field is most clearly visible. The material is seen to form clear striations, roughly perpendicular to the direction of the comet's motion. These striations are long-lived; the brightest was first detected in the 171 Å channel at 2011 December 15 23:57:47 UT and seen to persist until 2011 December 16 00:16:23 UT, almost 19 minutes, and 8 minutes after the comet went behind the solar limb.

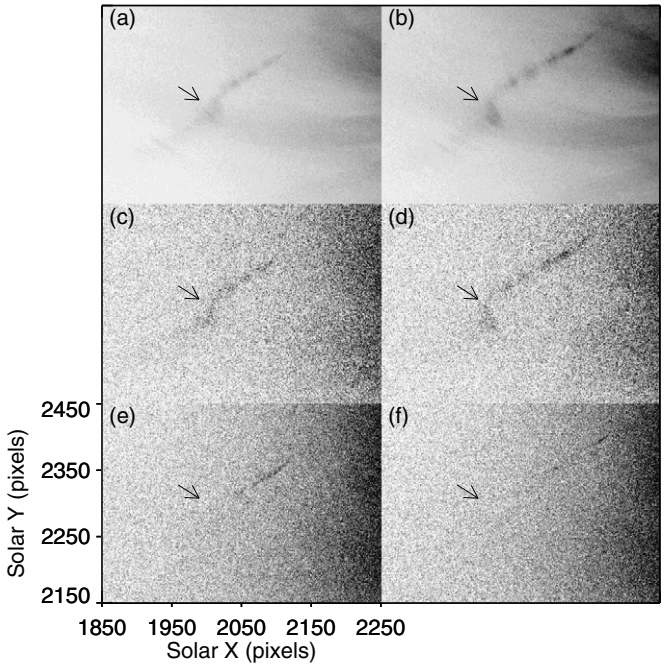

Figure 1. Emission from comet C/2011 W3 (Lovejoy) pre-perihelion. The color scale has been reversed, with darker colors indicating brighter emission. The comet is traveling up and to the right, toward the solar disk, which is to the extreme right of the images. All panels show the same location. Axes units are given in AIA pixels with (0, 0) being the bottom left of the full 4096×4096 AIA image. Panels (a) and (b) show emission from the 171 Å channel of AIA at 00:00:12 UT and 00:01:11 UT, respectively; panels (c) and (d) show the 131 Å channel at 00:00:10 UT and 00:01:10 UT, respectively; and panels (e) and (f) show the 304 Å channel at 00:00:08 UT and 00:01:08 UT, respectively. The arrow is at the same location in each image and indicates the kink in the tail described in the text.

Panels (c) and (d) of Figure 1 show the 131 Å observations at close to the same time as those of panels (a) and (b). The signal to noise is smaller than in the 171 Å passband, but the cometary emission is spatially similar. This is not the case for 304 Å emission, shown in panels (e) and (f). The emission shown in panel (e) is more spatially confined than that of panels (a) and (c). Comparing the emission at the later observation time shown in panel (f) with panels (b) and (d) makes this even more apparent. For ease of comparison across the images, we have highlighted with an arrow a point where the emission from the comet tail appears to kink due to the magnetic field of the corona. Sunward of this point, cometary material appears to move up and left as it follows the magnetic field. In contrast, the emitting material below the arrow moves down and right. We also note that there is no detectable signal in the 304 Å channel at this point at the time of these images.

The emission in the 171 and 131 Å channels is far longer-lived than that of 304 Å. Under normal quiet-Sun (QS) conditions, these three channels image plasma at $\log T$ (K) of 5.9, 5.6, and 4.7, respectively. The similarity in the emission from the 131 and 171 Å channels thus indicate a different ionization/excitation mechanism from the QS. We suggest a solution to this problem in Section 5.

The differences in the comets' detections clearly indicate that characteristics of the comet and viewing geometry significantly influence the intensity of EUV emission caused by their interaction with the solar atmosphere. It is our aim in this work to propose a mechanism whereby emission is possible;

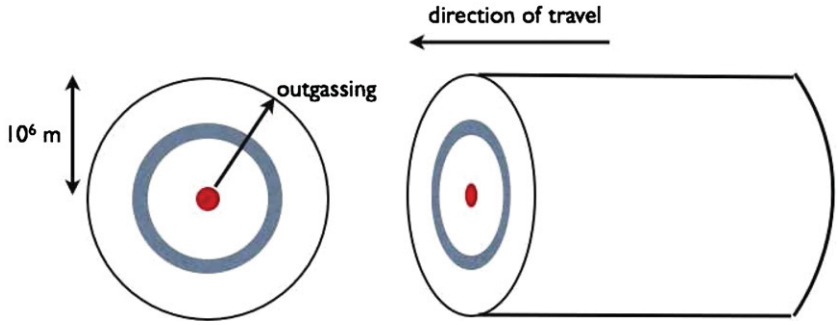

Figure 2. Schematic of the cometary emission model. The figure on the left shows the cross section perpendicular to the direction of motion. The figure on the right shows the comet trajectory as seen by AIA. The red dot in the center indicates the comet body. The blue area indicates one of the shells described in the text where a given ion exists.

(A color version of this figure is available in the online journal.)

characterizing the precise nature of the emission depends on an accurate knowledge of the cometary and coronal parameters.

3. EMISSION MODEL

As the comet approaches the Sun, material is sublimated from the comet surface. The mass-loss rate and the total mass of C/2011 N3 (SOHO) lost during the visibility in the AIA images are estimated to be $(0.01–1)\times10^{8}$ g s^{-1} and $(0.06–6)\times10^{10}$ g, respectively, by Schrijver et al. (2012).

We have constructed a simplified model that describes the evolution of the cometary material as it interacts with the solar atmosphere. We represent the comet coma as a cylinder along the direction of travel. A schematic representation is shown in Figure 2. The body of the comet is represented by the red circle with radius r_c at the center. We use $r_c = 50$ m, the upper limit of the nucleus radius given by Schrijver et al. (2012). The material sublimated from the surface then expands into the corona and forms the cylindrical geometry shown, with axis along the path of the comet's motion. The atoms that are formed in the coma become more highly ionized as they expand into the corona. We represent the space occupied by these ions as concentric shells (shown in blue in Figure 2) with inner radius r_1 and outer radius r_2. These radii are determined by the dissociation and ionization rates and the outgassing velocity.

The biggest failing of this model is that we do not take into account the magnetic field. Rather than a simple radial expansion, once the cometary material is ionized, it will be affected by the coronal magnetic field. As the level of ionization increases, the Larmor radius of the ions will decrease and the more highly charged species will form tighter spirals around the field lines. This is somewhat in opposition to the model presented here. The observations of C/2011 W3 (Lovejoy) clearly show that the cometary material is influenced by the coronal magnetic field, but whether the passage of the comet has any significant bearing on the underlying field has yet to be determined. Accounting for the magnetic field is not trivial and we leave such a study to a future work. However, the ions will move in a cylindrical pattern.

The precise composition of the material sublimated from the comet's surface is unknown. For the purposes of this work, we adopt the elemental abundances of Comet 1P/Halley (given in Table 1) from Delsemme (1988). H and O are the most abundant elements due largely to the presence of water ice in the comet and oxides being dominant in the asteroidal dust particles. Once it is deposited within the corona, H is rapidly ionized and thus does not contribute in any significant degree to the EUV emission.

Table 1
Elemental Abundance of Comet

Element	Fractional Abundance (Number)
H	0.484
C	0.137
N	0.023
O	0.304
Mg	0.011
Si	0.016
S	0.010
Fe	0.011

Note. Elemental abundances in Comet 1P/Halley (Delsemme 1988).

The most important elements to consider are O and Fe; O has a high abundance in the comet and many of the AIA channels cover wavelength ranges with strong Fe emission lines. To be as complete as possible, we have examined the eight most abundant elements of Comet 1P/Halley, i.e., those listed in Table 1—H, C, N, O, Mg, Si, S, and Fe. We will show that, of these, only O and Fe cause any significant emission in the AIA passbands.

There is some uncertainty in the outflow velocity from the surface; from the observations of C/2011 N3 (SOHO), we estimate the time taken for material to travel from the surface of the nucleus to the extent of the visible coma to be ∼60 s. Assuming the material flows radially from the nucleus at a constant velocity gives an outflow velocity of $v_{\rm out} = 17\,{\rm km\,s^{-1}}$. We explore the sensitivity of the model to this timescale by allowing it to vary from 10 to 90 s. The emission predicted by the model described here is dependent on the total time the cometary material remains emitting, rather than on the precise outflow velocity, so any influence of the magnetic field on the direction and magnitude of $v_{\rm out}$ will not greatly affect the model results if the emitting time remains unchanged. For comet C/2011 W3 (Lovejoy), however, emission is seen to persist for up to 20 minutes in certain AIA channels. The nature of this emission is somewhat different from the simplistic model presented here. It is seen to follow the solar magnetic field but, after the first minute of emission, does not appear to expand into the corona, rather maintaining consistent spatial dimensions before gradually fading from view. For this reason, we have chosen to use outflow velocities of $v_{\rm out} = 17\,{\rm km\,s^{-1}}$ for the emission calculations, but we make some comments on the extended duration of the C/2011 W3 (Lovejoy) emission in Section 5.

The comet perihelion parameter of $q = 0.0052986$ (Schrijver et al. 2012) for C/2011 N3 (SOHO) corresponds to a height above the solar surface of 97,200 km. Both comets were observed to pass through regions of low solar activity. Typical values for the QS electron temperature and density at this height are $T_e = 1.5 \times 10^6$ K and 10^8 cm^{-3}, respectively. We use these values throughout for the zone of interaction between the comet and the corona. In the absence of the comet, emission measured by AIA comes predominantly from lower in the atmosphere. When comparing observations of the comet with background QS emission, we use an average QS differential emission measure (DEM) from Vernazza & Reeves (1978) and an electron density of 5×10^8 cm^{-3}.

4. DISSOCIATION AND IONIZATION OF COMETARY MATERIAL

4.1. Dissociation

The sublimated molecules are 50% water by mass (Delsemme 1988). The destruction of these water molecules is mostly by photodissociation:

$$H_2O + h\nu \rightarrow OH + H + 3.42 \text{ eV} \quad (1)$$

$$\rightarrow H_2 + O(^1D) + 3.84 \text{ eV} \quad (2)$$

$$\rightarrow H + H + O + 0.7 \text{ eV} \quad (3)$$

$$\rightarrow H_2O^+ + e + 12.4 \text{ eV}. \quad (4)$$

The first of these reactions is the most likely, with a branching ratio of 86%. The reaction rate of this process at 1 AU is given by Combi et al. (2004) as 1.04×10^{-5} s^{-1} for the nonflaring Sun at medium activity. The rates given by Combi et al. (2004) are in broad agreement with those of previous work by Huebner et al. (1992). If we assume that this rate scales as the inverse square of the distance to the radiation source, then the photodissociation rate of the comet at the solar surface is $\sim 4.8 \times 10^{-1}$ s^{-1}. This translates to a lifetime of $\sim$2.08 s for a water molecule at the solar surface. At small heliocentric distances, thermally excited states in the molecule will increase the photodissociation rate such that the r^{-2} scaling is not entirely accurate. Our estimate of the lifetime is thus an upper limit (i.e., a lower limit of the rate constant).

The hydroxyl radical resulting from the dissociation of water will also photodissociate:

$$OH + h\nu \rightarrow O(^3P) + H + 1.27 \text{ eV} \quad (5)$$

$$\rightarrow O(^1D) + H + 7.90 \text{ eV} \quad (6)$$

$$\rightarrow O(^1S) + H + 9.80 \text{ eV} \quad (7)$$

$$\rightarrow OH^+ + e + 19.1 \text{ eV}. \quad (8)$$

To find the total rate for OH dissociating to O and H, we take the sum of the first three of these reactions. The total rate constant at 1 AU is given by Combi et al. (2004) as 2.5×10^{-5} s^{-1}. The resulting rate coefficient at the solar surface is then 1.2 s^{-1}, corresponding to a lifetime of 0.86 s. The mean time for a water molecule to dissociate to O and H can then be estimated as 2.9 s.

In addition to water, various other molecules are sublimated from the surface. Under typical solar conditions, most of the AIA channels are dominated by emission from Fe ions so we are interested in any Fe sublimated from the comet that may contribute to the emission detected by AIA. Fe I emission has been observed in the spectra of comet Ikeya–Seki (Preston 1967), most likely produced by ablation or vaporization of refractory grains. At the end stages of the asteroidal evaporation, the most important molecule containing Fe is ferrous oxide (FeO). The photodissociation cross section for FeO at 252 nm is 1.2×10^{-18} cm^2 (Chestakov et al. 2005). The solar flux at 1 AU is $\sim 5 \times 10^{12}$ photons cm^{-2} s^{-1} at 252 nm, so the rate at 1 AU is at least $\sim 6 \times 10^{-6}$ s^{-1}. At the solar surface this is 0.28 s^{-1}, or a lifetime of 3.6 s, i.e., comparable to that of water. Other molecules, such as MgO, will also rapidly photodissociate, adding another O atom to the cometary debris. However, the metallic ion so produced does not emit in the AIA passbands.

4.2. Ionization

The neutral atoms formed by dissociation are ionized through charge exchange with coronal protons, through impact with coronal electrons and protons, and by photoionization. We consider each of these processes in turn.

4.2.1. Charge Exchange

Electron capture by hydrogen ions due to collisions with neutral oxygen,

$$H^+ + O(^3P) \rightarrow H + O^+(^4S), \quad (9)$$

is a near-resonant reaction. Cross sections have been calculated by Stancil et al. (1999) for collision energies between 0.1 meV/u and 10 MeV/u. For a collision energy of 2 keV (corresponding to the energy of H^+ in the collision with the comet material), the rate coefficient for the reaction is 5.52×10^{-8}. For a coronal proton density of 10^8 cm^{-3}, the lifetime of cometary O atoms is thus 0.18 s. The reverse reaction is considerably less likely due to the negligible abundance of neutral H in the corona.

The resonant charge exchange process between H and protons,

$$H^+ + H(1s) \rightarrow H(1s) + H^+, \quad (10)$$

has been studied by Bates & Dalgarno (1953). They provide tabulated cross sections down to an impact energy of 2.5 keV. The cross section has a weak energy dependence and no other resonances at these energies, so we can extrapolate below this energy to find a cross section of $\sim 6 \times 10^{-15}$ cm^2 at an energy of 2 keV. For a coronal proton density of 10^8 cm^{-3} and a collision energy of 2 keV, this translates to a mean lifetime of only 0.027 s before cometary hydrogen atoms are ionized by charge transfer. As above, the inverse process is much less efficient because of the scarcity of neutral H in the corona.

During the initial expansion the density of H and O exceeds 10^8 cm^{-3}. This means the time to become ionized is increased until the comet material has expanded to a radius that includes sufficient protons to ionize all H and O. Until then, the situation is more complicated.

4.2.2. Electron-impact Ionization

Following the initial ionization of the neutral species, subsequent ionization is dominated by impact with free electrons of

Table 2
Ionization Rates for Selected Ions (s^{-1})

Ionization Level	CX	EII	Photoionization	PII	Total
$H \rightarrow H^{+}$	37.6	2.9	4.3×10^{-3}	...	40.5
$O \rightarrow O^{+}$	5.5	8.3	1.5×10^{-2}	4.2×10^{-1}	14.2
$O^{+} \rightarrow O^{2+}$	...	2.8	6.5×10^{-3}	3.1×10^{-4}	2.8
$O^{2+} \rightarrow O^{3+}$	...	1.2	1.4×10^{-3}	4.2×10^{-5}	1.2
$O^{3+} \rightarrow O^{4+}$	...	4.1×10^{-1}	5.1×10^{-5}	8.0×10^{-6}	4.1×10^{-1}
$O^{4+} \rightarrow O^{5+}$	...	1.1×10^{-1}	...	1.5×10^{-6}	1.1×10^{-1}
$O^{5+} \rightarrow O^{6+}$	...	3.4×10^{-2}	...	3.5×10^{-7}	3.4×10^{-2}
$Fe \rightarrow Fe^{+}$	...	20.6	8.4×10^{-2}	1.7	22.3
$Fe^{+} \rightarrow Fe^{2+}$	...	6.3	...	3.6×10^{-3}	6.3
$Fe^{2+} \rightarrow Fe^{3+}$	...	6.6	...	5.4×10^{-4}	6.6
$Fe^{3+} \rightarrow Fe^{4+}$	...	3.8	...	8.2×10^{-5}	3.8
$Fe^{4+} \rightarrow Fe^{5+}$	...	1.6	...	1.9×10^{-5}	1.6
$Fe^{5+} \rightarrow Fe^{6+}$	...	8.4×10^{-1}	...	5.5×10^{-6}	8.4×10^{-1}
$Fe^{6+} \rightarrow Fe^{7+}$	...	4.6×10^{-1}	...	1.9×10^{-6}	4.6×10^{-1}
$Fe^{7+} \rightarrow Fe^{8+}$	...	2.0×10^{-1}	...	6.8×10^{-7}	2.0×10^{-1}
$Fe^{8+} \rightarrow Fe^{9+}$	...	5.4×10^{-2}	...	3.0×10^{-7}	5.4×10^{-2}
$Fe^{9+} \rightarrow Fe^{10+}$	...	3.0×10^{-2}	...	1.7×10^{-7}	3.0×10^{-2}
$Fe^{10+} \rightarrow Fe^{11+}$	...	1.5×10^{-2}	...	9.5×10^{-8}	1.5×10^{-2}
$Fe^{11+} \rightarrow Fe^{12+}$	...	7.5×10^{-3}	...	4.8×10^{-8}	7.5×10^{-3}
$Fe^{12+} \rightarrow Fe^{13+}$	...	4.0×10^{-3}	...	2.6×10^{-8}	4.0×10^{-3}

Notes. Ionization rates of various processes at the solar surface. Charge exchange (CX), electron-impact ionization (EII), and proton-impact ionization (PII) rates are for an electron and proton density of 10^{8} cm^{-3}. Photoionization was not considered for states O^{4+} and higher, or Fe^{+} and higher.

the corona. We estimate the timescales of these reactions under the assumption that the electron velocity is large in comparison to that of the cometary ions. For a Maxwellian distribution of free electrons with temperature 1.5×10^{6} K, the mean electron velocity is

$$v_{e} = \sqrt{\frac{8kT_{e}}{\pi m_{e}}} \approx 7.6 \times 10^{3}\ \mathrm{km\,s^{-1}}, \tag{11}$$

so the free electrons in the corona are over an order of magnitude faster than the cometary oxygen ions. For comparison, coronal protons and oxygen ions have mean velocities of 1.8×10^{2} and 44 km s^{-1}, respectively. A proper analysis of the electron-impact ionization rate would consider an anisotropic electron velocity distribution in the rest frame of the ion. However, given the disparity in the velocity of the interacting electrons and ions, it is safe to proceed under the assumption of an isotropic Maxwellian electron distribution of $T_{e} = 1.5 \times 10^{6}$ K in the rest frame of the target ion.

To trace the ionization level of cometary oxygen as it passes through the corona, we consider the following reactions:

$$O^{q+} + e \rightarrow O^{(q+1)+} + e + e, \tag{12}$$

where q is the charge of the ion. We use the rate coefficients of Dere (2007), an electron temperature of 1.5×10^{6} K, and a density of 10^{8} cm^{-3} to derive reaction rates for this process. The results are summarized in Table 2.

From these results we can estimate which ionization stages of O will be sufficiently long-lived to contribute to EUV emission. If the plasma were allowed to relax to ionization equilibrium then the highest ionization stage reached under these conditions would be O^{6+} (Bryans et al. 2009). We thus expect to see emission from ionization stages up to and including $q = 6$. Given the ionization rates of the cometary material, this ionization state will be reached only after sufficient time has elapsed.

Dere (2007) also provides rate coefficients for the electron-impact ionization of Fe. We have given the rates for the first 12 ionization stages at an electron temperature of 1.5×10^{6} K and a density of 10^{8} cm^{-3} in Table 2. Analyzing these timescales shows that the highest ionization stage reached is Fe^{9+} for $v_{out} = 17\ \mathrm{km\,s^{-1}}$.

4.2.3. Photoionization

The photoionization rate of the dissociated atoms and ions is dependent on the solar EUV flux. The comet is exposed to a wide range of radiances as it travels close to the solar surface. For this reason, we choose to use the average EUV spectral irradiances at 1 AU from the *Thermosphere Ionosphere Mesosphere Energetics Dynamics* (*TIMED*) spacecraft's Solar EUV Experiment (SEE; Woods et al. 2005). Values between 2002 and 2011.5 were averaged to produce the irradiances used here. We use the cross sections from Verner & Yakovlev (1995) and Verner et al. (1996) to calculate the photoionization rates at 1 AU and have calculated the equivalent rate at the solar surface by scaling by r^{2}. The values are given in Table 2. In comparison to resonant charge exchange and electron-impact ionization, photoionization has a negligible impact on the ionization rate. A flare could have larger photoionization consequences, but none was observed during the perihelion passage of either of the comets discussed here. For this reason we have only listed the photoionization rate for the low charge states of O and Fe in Table 2.

Photoionization of neutral hydrogen also plays a role in the production of protons. According to Keller (1976), the calculated lifetime of cometary H atoms due to photoionization from the solar radiation field at a distance of 1 AU is 1.4×10^{7} s. This value is comparable to that from the *TIMED*/SEE irradiances, where the average photoionization lifetime over 2002–2011.5 was calculated as 1.1×10^{7} s at 1 AU. The resulting lifetime against photoionization at the solar surface is 2.4×10^{2} s.

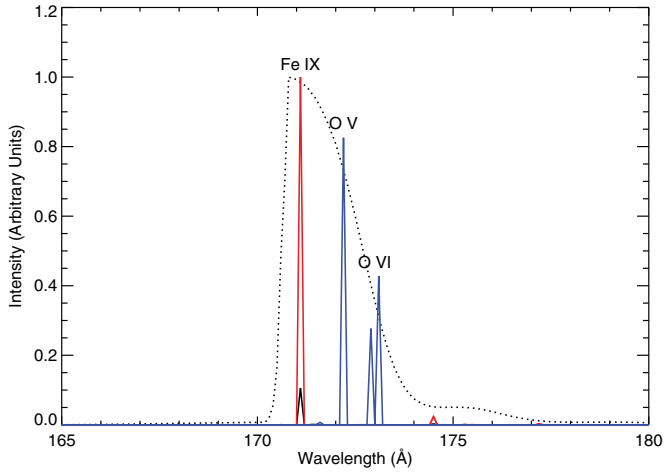

Figure 3. Emission from cometary ions in the bandpass of AIA 171 Å compared to QS. Fe emission from the comet is shown in red and O emission from the comet in blue. Black lines indicate a typical spectrum due to the QS. The dotted line is the effective area of the AIA passband. The colored lines are the spectrum from cometary O and Fe ions with outgassing velocity of 17 km s^{-1}. The strongest emission lines have been labeled.

(A color version of this figure is available in the online journal.)

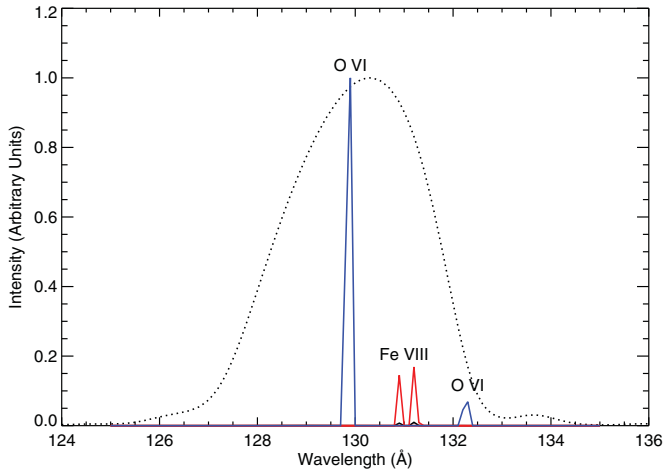

Figure 4. Same as Figure 3 but for 131 Å.

(A color version of this figure is available in the online journal.)

4.2.4. Ionization by Protons

The relative velocity of the cometary ions to the protons in the corona is ∼600 km s^{-1}. To calculate the rate of ionization due to impact with energetic protons, we use the classical approximation of Gryziński (1965). Results are shown in Table 2 for O and Fe. They are negligible compared to other ionization processes.

Cometary protons, resulting from sublimated water molecules that have been dissociated and subsequently ionized, will initially be traveling at the velocity of the comet relative to the corona. This velocity of 600 km s^{-1} corresponds to a proton beam of 2 keV. Can these fast protons cause ionization and excitation of the coronal plasma they are passing through? This is the same reaction as described above where fast cometary ions collide with slower coronal protons. Using the same approach, we can show that proton impact does not have a significant effect on the ionization balance of the plasma.

For it to be important, the proton-impact rate has to be comparable to the electron-impact ionization rate and the recombination rate. Taking ionization of O as an example, the

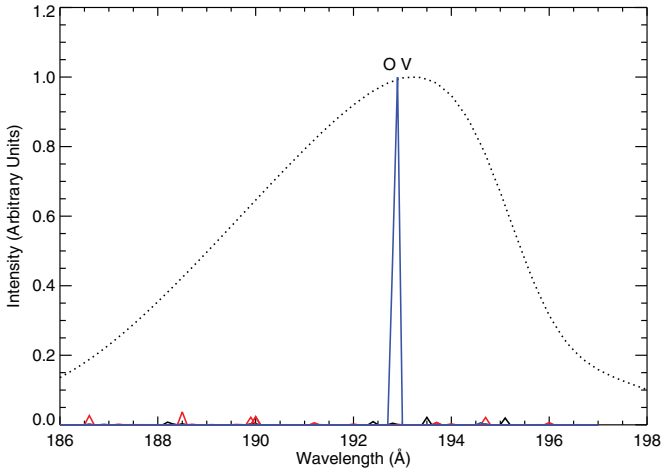

Figure 5. Same as Figure 3 but for 193 Å.

(A color version of this figure is available in the online journal.)

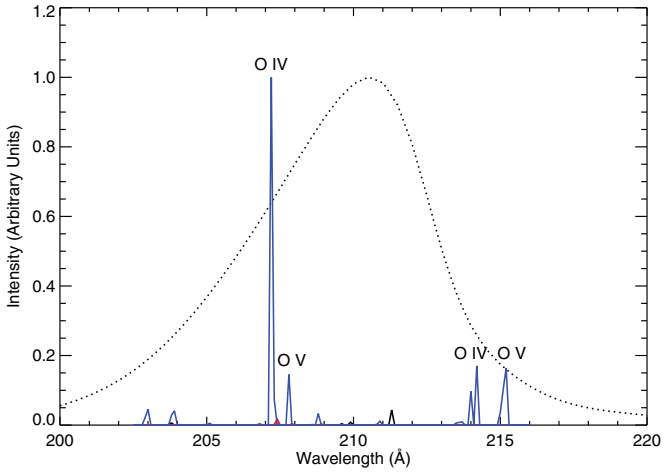

Figure 6. Same as Figure 3 but for 211 Å.

(A color version of this figure is available in the online journal.)

rate coefficient for proton impact is ∼5 orders of magnitude smaller than that for electron impact for the ions present in the corona (see Table 2). For the conditions outlined in Section 3 and the dissociation time for water given in Section 4.1, the highest proton density we can expect in the comet is ∼10^{11} cm^{-3}, only around three orders of magnitude greater than the coronal density. The ionization rate by proton impact is thus two orders of magnitude smaller than that by electron impact.

5. RESULTS

Using the physical conditions outlined in Section 3 and the ionization rates of Section 4.2, we have calculated the line emission from all elements listed in Table 1 in each AIA bandpass using CHIANTI (Dere et al. 1997, 2009). Collisional redistribution among the excited states of the ion is several orders of magnitude faster than ionization, so we have assumed detailed balance applies to the distribution of those energy levels. The results are shown in Figures 3–9 for an outflow time of 60 s. The intensities have been folded with the effective areas of the respective AIA filters (taken from SolarSoft; see also Boerner et al. 2012) and compared to the average QS emission. All intensities are integrated over the emitting area described in Section 3 and outlined in Figure 2 and compared with QS intensities over the same area. Of the elements considered

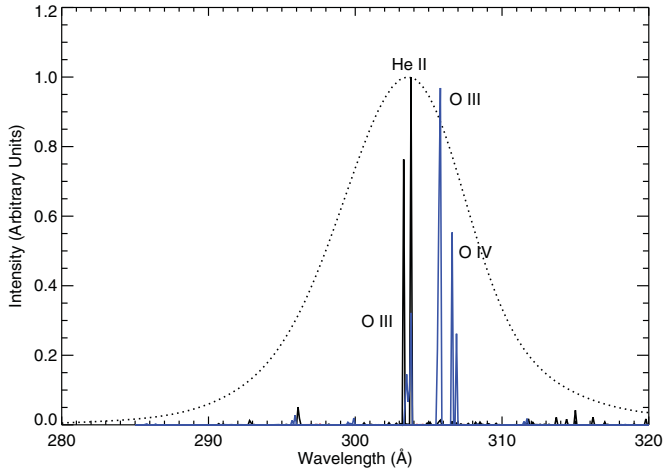

Figure 7. Same as Figure 3 but for 304 Å.

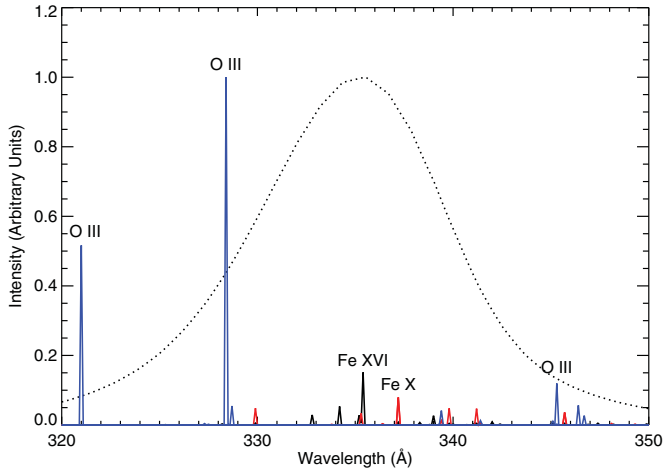

Figure 8. Same as Figure 3 but for 335 Å.

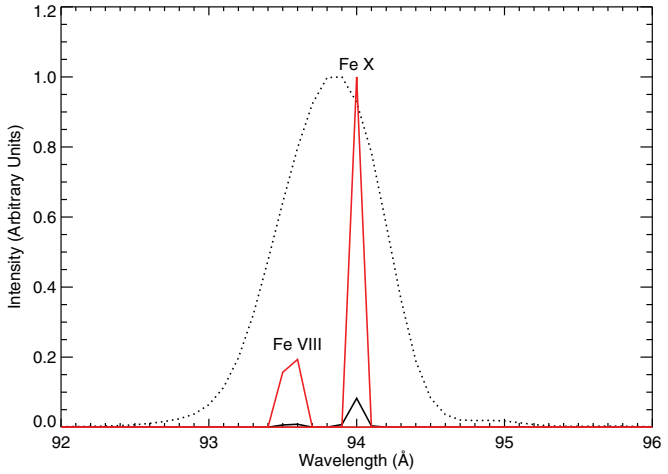

Figure 9. Same as Figure 3 but for 94 Å.

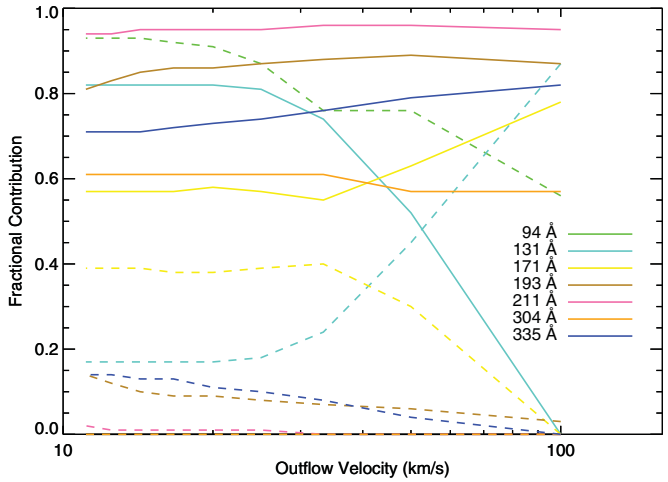

Figure 10. Intensity of O and Fe emission as a function of outflow velocity as detected by each AIA bandpass is given as a fraction of the total emission from the comet plus the average QS emission. The results are given for the conditions given in Section 3. Solid lines show the fractional contribution from cometary O ions and dashed lines from cometary Fe ions.

(H, O, C, N, Mg, Si, S, and Fe), only the ions of O and Fe contribute any significant emissions in the wavelength ranges of the AIA instrument.

We note here that the He II lines that dominate the QS emission in the 304 Å channel are not properly modeled by CHIANTI, which underestimates the observed intensities by a significant factor (see, e.g., Andretta et al. 2003). For this reason, we have multiplied the background QS emission from these lines by a factor of 20.0 to bring them in line with observation (Warren 2005).

For each AIA bandpass, we have calculated the fractional increase in radiance it would detect due to the cometary emission mechanism. We have integrated the emission over the wavelength range of each bandpass and compared the total intensity of the QS plus comet emission to QS emission alone. We have calculated the dependence of this fractional increase on the outflow velocity and show the results in Figure 10. The time for the cometary material to flow from the nucleus to the edge of the emitting region is allowed the range 10–90 s (an outflow velocity of 11–100 km s^{-1}). The solid lines show the contribution from O and the dashed lines show the contribution from Fe. The outflow velocity has an impact on the relative contribution from O and Fe ions to the emission spectra, most notably in the 131 and 171 Å passbands, but does not alter the total fraction of emission from cometary ions relative to the background to a significant degree.

Our model predicts emission in the 171 Å bandpass from O V, O VI, Fe IX, and a smaller contribution from Fe X. Under normal QS conditions this bandpass is dominated by Fe IX emission. The only other bandpass with significant emission from both O and Fe due to the cometary material is the 131 Å channel. Here, contributions to the emission come from O VI and Fe VIII. These same Fe VIII lines are those normally strongest in this channel under QS conditions. It is significant that the 171 and 131 Å channels are the only two that detect strong O VI emission lines. These are the highest ionization stages of O detectable in any of the AIA passbands, taking longer to form than the lower stages, and thus explaining the time delay in the observations from these channels (see Figure 1). We expand on this argument in Section 6.

In the 193, 211, 304, and 335 Å passbands, O emission dominates over Fe. A single O V line dominates the emission spectrum in the 193 Å passband. The 211 Å passband has contributions from a number of O IV and O V lines. O III and O IV are the strongest emitters in the 304 Å passband, and O III dominates the emission in the 335 Å passband. We note a progression of emission from O V, through O IV, to O III on advancing through the 193, 211, 304, and 335 Å passbands. We

return to this point in Section 6 when discussing a possible time lag in the observations from these channels.

The 94 Å passband has no O emission lines in its wavelength range. Here, emission from the comet material is from Fe VIII and Fe X and acts to increase the same emission lines that are strongest in the quiescent QS.

6. DISCUSSION AND CONCLUSIONS

We have shown that emission from the O and Fe atoms deposited in the corona by the passage of a comet is a viable mechanism to explain the increased radiance detected by AIA. The rapid injection of atoms to the corona followed by their ionization through successive ionization stages produces emission lines not normally present at coronal temperatures. The exact structure of the resulting spectra and their magnitude relative to the background corona are dependent on both the coronal and cometary parameters. Comparing our calculations with the AIA observations may provide a means of determining these parameters more accurately than has been possible heretofore.

The difference in the emission detected across the AIA channels for C/2011 W3 (Lovejoy) can be explained by our model if one considers the O emission. There is some observational evidence of the 304 and 335 Å channels showing emission only close to the comet nucleus but that does not persist. By contrast, the 131 and 171 Å channels show more spatially extended emission that persists for up to 20 minutes. The 304 Å channel has contributions from O III and O IV while 335 Å has strong contributions from O IV. According to our model, O will emit in these ionization stages for several seconds before being further ionized. Both 131 and 171 Å channels have significant contributions from O VI. This ion has a higher formation temperature, close to the ambient coronal temperature, and so remains present in the plasma for longer than the lower ionization stages. The observed fading must come from the diminution in the number density of oxygen nuclei in the field of view.

By a similar argument, the model presented here predicts that there should be a time lag in the emission from the AIA channels. This should follow the ionization stages of O that contribute to the emission in each wavelength channel, i.e., emission should first be detected in 335, followed by 304, then 211 and 193, and finally in 131 and 171 Å. Light curves of C/2011 W3 (Lovejoy) are being measured and the time lag between the channels is expected to be only a few seconds (see Table 2) so it remains to be seen whether observations spaced by 12 s can resolve any such time delay.

Estimates of several parameters influence the predicted emission to varying degrees. The assumed density of the corona through which the comet passes is particularly important. A larger density than that assumed here (10^8 cm^{-3}) would result in faster ionization and hence increased emission from higher ionization stages of O and Fe. The density assumed for the plasma responsible for the QS emission does not affect the cometary emission but will change the spectrum of the background corona that interferes with the detection of the comet. Finally, the density of the outgassing molecules will impact the relative intensity of the cometary and QS spectra. Within the range of reasonably expected conditions (around 1–2 $\times$ 10^6 K), the temperature assumed for the corona does not significantly alter the calculated spectra.

Our model assumes that the cometary species move radially away from the nucleus of the comet after sublimating. This assumption neglects the influence of the magnetic field on the ions. The primary effect of the gyrorotation will be an increase in the effective path length of the ions as they spiral along the field lines. A proper analysis would require the direction and magnitude of the magnetic field, and is beyond the scope of this work, but is worth further study.

Intensity profiles from AIA channels also show indications of absorption by the denser inner regions of the comet's coma when viewed against the disk of the Sun (Schrijver et al. 2012). The model presented here may be able to account for this. Near the comet surface, ions have yet to be ionized to the stages responsible for the emission seen later in the AIA observations. It is possible that the lower ionization stages cause absorption in this region and the relative brightness may track the O I photoionization curve. We intend to explore this possibility in future work.

Research was supported by the *Solar Dynamics Observatory*. We acknowledge many helpful comments and suggestions from K. Battams, J. C. Brown, H. S. Hudson, W. Liu, P. Saint-Hilaire, and C. J. Schrijver.

REFERENCES

Andretta, V., Del Zanna, G., & Jordan, S. D. 2003, A&A, 400, 737
Bates, D. R., & Dalgarno, A. 1953, Proc. Phys. Soc. A, 66, 972
Biesecker, D. A., Lamy, P., Cyr, O. C. St., Llebaria, A., & Howard, R. A. 2002, Icarus, 157, 323
Boerner, P., Edwards, C., Lemen, J., et al. 2012, Sol. Phys., 275, 41
Brown, J. C., Potts, H. E., Porter, L. J., & Le Chat, G. 2011, A&A, 535, A71
Brueckner, G. E., Howard, R. A., Koomen, M. J., et al. 1995, Sol. Phys., 162, 357
Bryans, P., Landi, E., & Savin, D. W. 2009, ApJ, 691, 1540
Chestakov, D. A., Parker, D. H., & Baklanov, A. V. 2005, J. Chem. Phys., 122, 084302
Combi, M. R., Harris, W. M., & Smyth, W. H. 2004, in Comets II. Gas Dynamics and Kinetics in the Cometary Coma: Theory and Observations, ed. M. C. Festou, H. U. Keller, & H. A. Weaver (Tucson, AZ: Univ. Arizona Press), 523
Cravens, T. E. 1997, Geophys. Res. Lett., 24, 105
Delsemme, A. H. 1988, Phil. Trans. R. Soc. A, 325, 509
Dennerl, K., Englhauser, J., & Trumper, J. 1997, Science, 277, 1625
Dere, K. P. 2007, A&A, 466, 771
Dere, K. P., Landi, E., Mason, H. E., Monsignori Fossi, B. C., & Young, P. R. 1997, A&AS, 125, 149
Dere, K. P., Landi, E., Young, P. R., et al. 2009, A&A, 498, 915
Domingo, V., Fleck, B., & Poland, A. I. 1995, Sol. Phys., 162, 1
Green, D. W. E. 2011, CBET, 2930
Gryziński, M. 1965, Phys. Rev., 138, 336
Gundlach, B., Blum, J., Skorov, Y. V., & Keller, H. U. 2012, arXiv:1203.1808
Huebner, W. F., Keady, J. J., & Lyon, S. P. 1992, Ap&SS, 195, 1
Keller, H. U. 1976, Space Sci. Rev., 18, 641
Knight, M. M., A'Hearn, M. F., Biesecker, D. A., et al. 2010, AJ, 139, 926
Krasnopolsky, V. 1997, Icarus, 128, 368
Lemen, J. R., Title, A. M., Akin, D. J., et al. 2012, Sol. Phys., 275, 17
Lisse, C., Dennerl, K., Englhauser, J., et al. 1996, Science, 274, 205
Marsden, B. G. 2005, ARA&A, 43, 75
Pesnell, W. D., Thompson, B. J., & Chamberlin, P. C. 2012, Sol. Phys., 275, 3
Preston, G. W. 1967, ApJ, 147, 718
Schrijver, C. J., Brown, J. C., Battams, K., et al. 2012, Science, 335, 324
Sekanina, Z. 1984, Icarus, 58, 81
Sekanina, Z. 2003, ApJ, 597, 1237
Sekanina, Z., & Chodas, P. W. 2012, ApJ, 757, 127
Stancil, P. C., Schultz, D. R., Kimura, M., et al. 1999, A&AS, 140, 225
Vernazza, J. E., & Reeves, E. M. 1978, ApJS, 37, 485
Verner, D. A., Ferland, G. J., Korista, K. T., & Yakovlev, D. G. 1996, ApJ, 465, 487
Verner, D. A., & Yakovlev, D. G. 1995, A&AS, 109, 125
Warren, H. P. 2005, ApJS, 157, 147
Weissman, P. R. 1983, Icarus, 55, 448
Woods, T. N., Eparvier, F. G., Bailey, S. M., et al. 2005, J. Geophys. Res. (Space Phys.), 110, 1312